Original Article

MOLECULAR METABOLISM

Adiponectin release and insulin receptor targeting share *trans*-Golgi-dependent endosomal trafficking routes

Maria Rödiger [1,2], Martin W. Werno [1,2], Ilka Wilhelmi [1,2], Christian Baumeier [1,2], Deike Hesse [1,2], Nina Wettschureck [3], Stefan Offermanns [3], Kyungyeun Song [4], Michael Krauß [4], Annette Schürmann [1,2,*]

ABSTRACT

Objective: Intracellular vesicle trafficking maintains cellular structures and functions. The assembly of cargo-laden vesicles at the *trans*-Golgi network is initiated by the ARF family of small GTPases. Here, we demonstrate the role of the *trans*-Golgi localized monomeric GTPase ARFRP1 in endosomal-mediated vesicle trafficking of mature adipocytes.

Methods: Control (*Arfrp1*$^{flox/flox}$) and inducible fat-specific *Arfrp1* knockout (*Arfrp1*$^{iAT-/-}$) mice were metabolically characterized. *In vitro* experiments on mature 3T3-L1 cells and primary mouse adipocytes were conducted to validate the impact of ARFRP1 on localization of adiponectin and the insulin receptor. Finally, secretion and transferrin-based uptake and recycling assays were performed with HeLa and HeLa M-C1 cells.

Results: We identified the ARFRP1-based sorting machinery to be involved in vesicle trafficking relying on the endosomal compartment for cell surface delivery. Secretion of adiponectin from fat depots was selectively reduced in *Arfrp1*$^{iAT-/-}$ mice, and *Arfrp1*-depleted 3T3-L1 adipocytes revealed an accumulation of adiponectin in Rab11-positive endosomes. Plasma adiponectin deficiency of *Arfrp1*$^{iAT-/-}$ mice resulted in deteriorated hepatic insulin sensitivity, increased gluconeogenesis and elevated fasting blood glucose levels. Additionally, the insulin receptor, undergoing endocytic recycling after ligand binding, was less abundant at the plasma membrane of adipocytes lacking *Arfrp1*. This had detrimental effects on adipose insulin signaling, followed by insufficient suppression of basal lipolytic activity and impaired adipose tissue expansion.

Conclusions: Our findings suggest that adiponectin secretion and insulin receptor surface targeting utilize the same post-Golgi trafficking pathways that are essential for an appropriate systemic insulin sensitivity and glucose homeostasis.

Keywords Adiponectin; ARFRP1; Exocytosis; Insulin receptor; *trans*-Golgi

1. INTRODUCTION

An appropriate adipose tissue function is a major determinant of metabolic health. Beside storage and supply of energy, the adipose tissue possesses a secretory capacity releasing a variety of bioactive molecules into the circulation, such as adipokines, cytokines, and lipid metabolites. To meet these secretory requirements, adipocytes crucially rely on a sophisticated vesicle trafficking machinery. However, despite that there is substantial knowledge about physiological effects of secreted factors, such as leptin and adiponectin, precise intracellular trafficking pathways and particular molecular components mediating the targeting and release of bioactive molecules are still largely elusive. Within the classical secretory pathway, transmembrane and soluble cargos travel *via* the endoplasmic reticulum (ER) and Golgi apparatus *en* route to their final destinations [1]. However, at a post-Golgi level, trafficking routes can diverge. In this context, the *trans*-Golgi network (TGN) is conventionally regarded as the main cargo sorting station; together with a broad range of accessory proteins, the TGN regulates accurate packaging of cargo into the right transport vesicle and delivery along correct trafficking routes. The assembly of cargo-laden vesicles at the TGN is initiated by the ARF family of small GTPases consisting of ARF, SAR (secretion-associated and Ras-related), and ARL (ARF-like) proteins [2]. Mammalian cells possess 6 ARF proteins and more than 20 ARF-like proteins, whose intracellular roles are poorly understood [3]. Among them, ARFRP1 (ADP-ribosylation factor-related protein 1), which localizes in the activated GTP-bound form to the TGN, has been functionally implicated in vesicle trafficking of VSVG (vesicular stomatitis virus G) [4,5], E-cadherin [6], Vangl2 (vang-like 2)

[1]Department of Experimental Diabetology, German Institute of Human Nutrition Potsdam-Rehbruecke (DIfE), 14558 Nuthetal, Germany [2]German Center for Diabetes Research, München-Neuherberg, 85764 Neuherberg, Germany [3]Department of Pharmacology, Max Planck Institute for Heart and Lung Research, 61231 Bad Nauheim, Germany [4]Department of Molecular Pharmacology and Cell Biology, Leibniz-Forschungsinstitut für Molekulare Pharmakologie (FMP), 13125 Berlin, Germany

*Corresponding author. German Institute of Human Nutrition Potsdam-Rehbruecke, Department of Experimental Diabetology, Arthur-Scheunert-Allee 114-116, 14558, Nuthetal, Germany. Fax: +49 0 33200 88 2334.

E-mails: Maria.Roediger@dife.de (M. Rödiger), Martin.Werno@dife.de (M.W. Werno), Ilka.Wilhelmi@dife.de (I. Wilhelmi), Christian.Baumeier@dife.de (C. Baumeier), deike.hesse-wilting@hu-berlin.de (D. Hesse), Nina.Wettschureck@mpi-bn.mpg.de (N. Wettschureck), Stefan.Offermanns@mpi-bn.mpg.de (S. Offermanns), Song@fmp-berlin.de (K. Song), Krauss@fmp-berlin.de (M. Krauß), schuermann@dife.de (A. Schürmann).

Received November 14, 2017 • Accepted November 18, 2017 • Available online 22 November 2017

https://doi.org/10.1016/j.molmet.2017.11.011

[7], and the glucose transporters GLUT4 [8] and GLUT2 [9]. Furthermore, conditional adipocyte-specific deletion of *Arfrp1* resulted in a severe lipodystrophic phenotype of newborn mice underlining the pivotal role of ARFRP1 for the development of functional adipose tissue depots [10].

To explore the impact of ARFRP1 as part of the vesicle trafficking machinery on the secretory capacity of mature adipocytes, we generated a mouse model with an inducible fat-specific disruption of the *Arfrp1* gene (*Arfrp1*$^{iAT-/-}$). Here, we demonstrate that the loss of *Arfrp1* from differentiated adipocytes diminishes adiponectin secretion and plasma membrane localization of the insulin receptor associated with detrimental effects on adipocyte metabolism and glucose homeostasis. These findings were attributed to defective endosomal-mediated exocytosis that was monitored *in vitro* following *Arfrp1* suppression.

2. MATERIAL AND METHODS

2.1. Animals

In order to generate inducible adipocyte-specific *Arfrp1* knockout animals on a C57BL/6J background, transgenic mice carrying floxed *Arfrp1* alleles (*Arfrp1*$^{flox/flox}$, N_{10} generation) [6] were crossed with mice heterozygously expressing the CreER^{T2}-transgene [11] under the control of the adipocyte-specific adiponectin promotor (*Adipoq*CreER^{T2}, kindly provided by Prof. Dr. Stefan Offermanns, MPI, Bad Nauheim) [12]. Mice were kept at a temperature of 22 ± 2 °C with a 12:12 h light–dark cycle and *ad libitum* access to drinking water and phytoestrogen-reduced standard diet (V1554-000 R/M–H, Ssniff). At 5 weeks of age, male *Arfrp1*$^{iAT-/-}$ and *Arfrp1*$^{flox/flox}$ mice received tamoxifen (1 mg/d, Sigma–Aldrich) by oral gavage for 5 consecutive days continued by feeding a tamoxifen-containing, phytoestrogen-reduced standard diet (400 mg/kg tamoxifen D.CRTAM400.R1, LASvendi GmbH) until the end of the study (7 or 10 weeks of age). This resulted in adipocyte-specific disruption of the *Arfrp1* gene in *Arfrp1*$^{iAT-/-}$ mice. All animal experiments were approved by the ethics committee of the State Office of Environment, Health and Consumer Protection (Federal State of Brandenburg, Germany).

2.2. Body composition, blood glucose, pyruvate tolerance test (PTT), and insulin response

Body composition of inducible adipocyte-specific *Arfrp1* knockout mice (*Arfrp1*$^{iAT-/-}$) and control littermates (*Arfrp1*$^{flox/flox}$) was determined weekly by nuclear magnetic resonance (EchoMRITM-100H, EchoMRI LCC). Blood glucose levels were measured using a CONTOUR® XT glucometer (Bayer). For PTT, 10-week-old mice were starved overnight (18 h) before receiving an i.p. injection of sodium pyruvate (2 g/kg of body weight; Sigma–Aldrich). Blood glucose levels were measured at indicated time points. For determination of insulin response in peripheral tissues, 10-week-old mice were fasted for 6 h before i.p.-injected with either insulin (1 IU/kg body weight, Actrapid®, Novo Nordisk) or an equal volume of vehicle (physiologic saline, Fresenius Kabi). After 20 min, mice were sacrificed and designated tissues collected for western blot analysis of phosphorylated and total AKT levels.

2.3. *Ex vivo* secretion and lipolysis assay

Gonadal (gon) and subcutaneous (sc) white adipose tissue (WAT) depots were removed from 7-week-old *Arfrp1*$^{iAT-/-}$ and *Arfrp1*$^{flox/flox}$ mice, rinsed in prewarmed PBS, minced into small pieces (~10 mg), and incubated in phenolred-free DMEM (PAN-Biotech) supplemented with 4.5 g/l glucose, 25 mmol/l HEPES, 1 mmol/l sodium pyruvate, 4 mmol/l glutamine, 1% penicillin/streptomycin, and 2% fatty acid-free BSA at 37 °C and 5% CO_2 for 24 h. Thereafter, supernatants were collected, centrifuged (500 *g* for 5 min), and analyzed for adiponectin and leptin concentration. To measure *ex vivo* lipolysis rates, gonWAT explants were incubated in the above-mentioned medium in the absence (basal lipolysis) or presence (stimulated lipolysis) of 10 μmol/l isoproterenol (Sigma–Aldrich) together with 1 μmol/l insulin (Roche) when indicated for 2 h before detection of non-esterified fatty acids (NEFA) in the supernatant. Fat explants were washed, collected and lyzed for protein measurement. Adipokine and NEFA levels were normalized to respective fat explant protein concentration.

2.4. Plasma and supernatant analyses

Designated adipokines were quantitatively assessed in plasma and supernatant of fat explants using respective ELISA kits (DY1119, MOB00, DY5430-05, DY1069, MWSP10, DY954, R&D Systems GmbH) following the manufacturer's instructions. Triglyceride, glycerol (TR0100, Sigma–Aldrich), and NEFA (NEFA-HR(2), Wako Chemicals GmbH) levels were measured in plasma and fat explant supernatant according to manufacturer's protocol.

2.5. Subcellular fractionation of primary and 3T3-L1 adipocytes

Subcellular fractionation of isolated primary adipocytes from gonWAT of 7-week-old *Arfrp1*$^{iAT-/-}$ and *Arfrp1*$^{flox/flox}$ mice (5–6 mice pooled per genotype) as well as 3T3-L1 adipocytes transfected with *nt*- (non-targeting) or *Arfrp1*-siRNA was performed as described before [13].

2.6. Protein extraction and western blotting

Tissue lysates were prepared using RIPA buffer [50 mM Tris–HCl (pH 7.2), 150 mM NaCl, 1 mM EDTA, 0.25% sodium deoxycholate, 1% Triton X-100, 2 mM Na_3VO_4] supplemented with phosphatase inhibitor (PhosSTOP, Roche) and protease inhibitor (cOmplete, Roche). Protein concentration was measured using Pierce BCA Protein Assay Kit (Thermo Scientific) according to the manufacturer's protocol. Western blot analysis of lysates and fractions from mouse tissue or 3T3-L1 adipocytes was performed as described previously [14]. The following primary antibodies were applied overnight at 4 °C: ARFRP1 (1:500; Abcam, ab108199), insulin receptor β subunit (IRβ; 1:500; Merck Millipore, GR36), IRS-1 (1:500; Cell Signaling, 3407), IRS-2 (1:500; Merck Millipore, MABS15), AKT (1:1,000; Cell Signaling, 9272), pAKT (Ser473; 1:1,000; Cell Signaling, 9271), AMPKα (1:1,000; Cell Signaling, 2532), pAMPKα (Thr172; 1:1,000; Cell Signaling, 2535), tFOXO (1:1,000, Cell Signaling, 2880S), pFOXO (1:1,000, Cell Signaling 9464S), adiponectin (1:500; Abcam, ab3455), calnexin (1:2,000; Abcam, ab22595), Rab11 (1/1,000; Thermo Fisher Scientific, 71–5300), α-tubulin (1:500; Sigma–Aldrich, T6199), and GAPDH (1:10,000; Ambion, AM4300). For non-denaturing western blot analysis of adiponectin isoforms, equal volumes of murine plasma samples were pre-diluted (1:30) and mixed with 2× adiponectin sample buffer [3% SDS, 20% Glycerol, 50 mM Tris, 0.02% Bromophenol blue) before incubation at room temperature for 1 h and separation in a precast gradient gel (4–15% Ready Gel Tris–HCl Gel, Bio-Rad). Corresponding HRP-conjugated secondary antibodies (Dianova) were applied (1:20,000) for 1 h at room temperature before targeted proteins were visualized using Amersham ECL Western Blotting Detection kit (GE Healthcare).

2.7. Histology

Adipose tissue depots were fixed in 4% formaldehyde and embedded in paraffin. Sections (2 μm) were deparaffinized, rehydrated, and stained with hematoxylin and eosin (H&E) using a standard protocol before dehydrated and mounted. Microscopic analysis was performed

with the Keyence BZ-9000 Fluorescence Microscope and corresponding BZ-II Analyzer software (Keyence International). Adipocyte area of 3 histological images per animal and 3–5 mice per genotype and age were assessed by applying an automated image analysis software (WimAdipose, Wimasis GmbH).

2.8. RNA extraction and quantitative real-time PCR (qRT-PCR)

Total RNA from mouse tissues was extracted using RNeasy Mini Kit (QIAGEN) according to manufacturer's instructions. RNA samples were reverse transcribed using the Moloney Murine Leukemia Virus Reverse Transcriptase (M-MLV RT, Promega). Gene expression levels were detected applying TaqMan Gene Expression Assays (*Arfrp1* Mm01220415_g1, *Adipoq* Mm00456425_m1; *G6pc* Mm00839363_m1, *Pck1* Mm01247058_m1, *Eef2* Mm01171434_g1) by using the LightCycler® 480 II/384 (Roche). Target gene expression was normalized to *Eef2* used as endogenous control.

2.9. Cell culture and si-RNA transfection

All cell lines were kept at 37 °C and 5% CO_2. 3T3-L1 cells (ATTC® CL-173™) were cultured in IMDM (4.5 g/l glucose, PAN-Biotech) supplemented with 10% newborn calf serum (NCS, PAN-Biotech). Differentiation of confluent cells was induced by applying IMDM including 10% fetal bovine serum (FBS, PAN-Biotech), 1.2 μg/ml insulin (Roche), 0.5 mM 3-isobutyl-1-methylxanthine (IBMX, Sigma–Aldrich), 0.25 μM dexamethasone (Sigma–Aldrich) and 2 μM rosiglitazone (Sigma–Aldrich). At day 3 and day 4 medium was replaced by IMDM containing 10% FBS and 1.2 μg/ml insulin. Transfection with indicated siRNAs was performed by electroporation at day 6 as previously described [10], and cells were cultivated for further 96 h before used in different experimental setups. HeLa (ATTC®) and HeLa M-C1 cells were cultured in DMEM (4.5 g/l glucose, Life Technologies) containing 10% FCS and 50 μg/ml penicillin/streptomycin. When reaching 40% confluency, cells were transfected with designated siRNAs by using Oligofectamine (LifeTechnologies) according to manufacturer's instructions, re-seeded on matrigel-coated (BD-Bioscience) coverslips the following day, and cultured for further 24 h before used in immunofluorescence-based assays.

2.10. HeLa M-C1 secretion assay

For monitoring constitutive secretion, transfected HeLa M-C1 cells [15] were washed with PBS and treated with 1 μM D/D solubilizer (Clontech) diluted in Hank's Balanced Salt Solution (HBSS, Gibco) to initiate secretion of the reporter. At the indicated time points, cells were placed on ice, washed twice with ice-cold PBS including 10 mM $MgCl_2$, and fixed with 4% paraformaldehyde (PFA) for 20 min at room temperature. GFP intensity was quantified per cell, and all time points were normalized to respective 0 min reflecting whole amount of reporter located within the ER.

2.11. Transferrin recycling

Transfected HeLa cells and 3T3-L1 adipocytes were serum-starved for 1 h and incubated with 15 μg/ml Alexa568-labeled transferrin (Alexa568-Tf, Life Technologies) at 37 °C for 30 min to saturate receptor-ligand uptake and recycling. After being washed with ice cold phosphate-buffered saline (PBS) containing 10 mM $MgCl_2$, cells were acid washed at pH 5.3 (0.1 M Na-acetate, 0.5 M NaCl) for 1 min on ice to remove surface-bound Tf (referred to 0 min), followed by washing with ice cold PBS/$MgCl_2$ and incubation with 1 mg/ml unlabeled Tf (Sigma–Aldrich) at 37 °C for 20 min to allow receptor-ligand exocytosis. Cells were fixed after 0 and 20 min with 4% PFA for 45 min at room temperature. Alexa568-Tf intensity was quantified per cell and the relative amount of released Tf was calculated as a measure of Tf–TfR exocytosis. For quantification of subcellular Tf–TfR localization, cells incubated with Alexa568-Tf at 37 °C for 30 min were classified into the following groups: overlapping Tf–TfR signals distributed throughout the entire cell (whole cell), primarily in the perinuclear region (perinuclear) or at the cell periphery (tip). Counted cells per classification were expressed as percentage of total number of cells.

2.12. Transferrin surface labeling and uptake

Transfected HeLa cells and 3T3-L1 adipocytes were serum-starved for 2 h and incubated with 15 μg/ml Alexa568-Tf for 50 min at 4 °C to block endocytosis. One set of cells was washed with ice cold PBS/$MgCl_2$ and fixed with 4% PFA for 45 min at room temperature to determine surface-bound Alexa568-Tf as a measure of TfR surface localization. Another set of cells was transferred to 37 °C for 5 min allowing Tf–TfR endocytosis, followed by washing with PBS/$MgCl_2$ and fixation with 4% PFA for 45 min at room temperature. Alexa568-Tf intensity was quantified per cell and the rate of endocytosis was calculated by the ratio of Tf uptake to Tf surface.

2.13. Immunocytochemistry

For immunocytochemical stainings of 3T3-L1 adipocytes, cells were serum-starved for 4–6 h, fixed with 4% PFA for 10 min, rinsed with PBS, washed with 50 mM NH_4Cl (Roth) and subsequently permeabilized for 6 min with 0.2% saponin (Sigma–Aldrich). After being washed with 0.02% saponin, cells were incubated for 30 min in blocking solution (2% BSA (Sigma–Aldrich) in 0.02% saponin) before application of primary antibodies diluted in blocking solution overnight at 4 °C. The following primary antibodies were used: ARFRP1 (1:100; Abcam, ab108199), insulin receptor β subunit (1:50; Merck Millipore, GR36), Rab11 (1:50; Thermo Fisher Scientific, 71-5300), γ-adaptin (1:100; BD Transduction Lab, 610385), LAMP1 (1:50; Abcam, [H4A3] ab25630), leptin (1:1000, anti-rabbit, self-made), adiponectin (1:100; Abcam, ab3455, ab22554), caveolin-1 (1:100; BD Transduction Lab, 610059). Thereafter, cells were incubated with corresponding AlexaFluor-labeled secondary antibodies (1:200; Thermo Fisher Scientific) and DAPI (1:1,000,000; Roche) diluted in blocking solution for 1 h at room temperature, followed by washing with 0.02% saponin and mounting using Fluorescence Mounting Medium (Dako). Imaging and quantification was performed with the Leica TCS SP8 X Laser Scanning Confocal Microscope (Leica Microsystems) and the corresponding image analysis software (Leica Application Suite X version 1.81).
Staining of fixed HeLa and HeLa M-C1 cells was performed as described in [16] using the following primary antibodies: ARFRP1 (1:200; Abcam, ab108199), transferrin receptor (1:300; Life Technologies, 13–6800), GM130 (1:100; BD Transduction Lab, 610822) and AlexaFluor-labeled secondary antibodies (1:200; Life Technologies). Cells were mounted using Immu-Mount (Thermo Fisher Scientific) including 10 μg/ml DAPI (Life Technologies). Stainings were analyzed and quantified using a spinning disc confocal microscope (Ultraview ERS, Perkin Elmer) with Volocity imaging software (Improvision, Perkin Elmer).

2.14. Statistical analysis

All data are reported as mean ± SEM of at least three different experiments, except when otherwise indicated. To compare differences between two groups, paired or unpaired Student's *t*-test or were performed. Differences between two groups over the time were evaluated using two-way ANOVA with Bonferroni's correction for multiple comparisons. Statistical analysis was performed with Prism 5 (GraphPad). Significance was accepted at $*P \leq 0.05$, $**P \leq 0.01$, $***P \leq 0.001$.

3. RESULTS

3.1. Adipocyte-specific deletion of *Arfrp1* selectively reduces adiponectin and adipsin secretion

As our previous studies have shown that the monomeric GTPase ARFRP1 regulates intracellular trafficking of certain cargo molecules and is indispensable for proper adipose tissue development, we aimed to clarify the role of ARFRP1 on secretory processes in mature adipocytes. We specifically deleted *Arfrp1* in adipocytes by tamoxifen treatment of 5-week-old *Arfrp1*$^{flox/flox}$ × *Adipoq*CreER^{T2} offspring mice. As shown in Figure S1 tamoxifen treatment resulted in a specific suppression of *Arfrp1* expression in adipose tissues, other organs were not affected. Two weeks following initiation of gene deletion, we screened for the abundance of different adipokines in the plasma of 7-week-old control (*Arfrp1*$^{flox/flox}$) and inducible adipocyte-specific *Arfrp1* knockout (*Arfrp1*$^{iAT-/-}$) mice. Levels of adiponectin as well as adipsin were significantly reduced in the circulation of mice lacking *Arfrp1* in adipose tissue depots, whereas other adipokines such as leptin and resistin were not affected (Figure 1A). As multimerization of adiponectin is described to be important for its secretion [17], we assessed the three multimeric forms of adiponectin by non-denaturing western blot analysis and observed similarly decreased abundance of all three isoforms in the plasma of *Arfrp1*$^{iAT-/-}$ compared to control mice (Figure 1B). Intriguingly, adiponectin transcript levels (*Adipoq*) determined in gonadal and subcutaneous white adipose tissue (gonWAT, scWAT) and in brown adipose tissue (BAT) were not altered between the genotypes (Figure 1C), indicating that ARFRP1 acts on the level of adiponectin secretion rather than influencing its expression. In addition, adiponectin and leptin secretion was measured *ex vivo* from gonWAT and scWAT explants generated from 7-week-old *Arfrp1*$^{iAT-/-}$ mice and control littermates. Consistent with *in vivo* results, adiponectin released from fat explants of *Arfrp1*$^{iAT-/-}$ animals was significantly lower than from those of control mice (gonWAT 55% and scWAT 59% of controls) (Figure 1D), whereas leptin release was not different between the genotypes (Figure 1E). Thus, these data reveal that ARFRP1 is specifically required for an appropriate adiponectin secretion.

3.2. Loss of *Arfrp1* leads to endosomal accumulation of adiponectin

In order to define the subcellular distribution of adiponectin, isolated adipocytes from gonWAT of 7-week-old *Arfrp1*$^{flox/flox}$ and *Arfrp1*$^{iAT-/-}$ mice as well as 3T3-L1 adipocytes transfected with *nt* (non-targeting)- or *Arfrp1*-siRNA were fractionated *via* differential centrifugation into subcellular compartments. Purity of the different fractions was assessed by respective marker proteins, e.g. SNAP23 for plasma membranes (Figure S2). In accordance with the defective secretion of adiponectin, it accumulated in the HDM fraction, containing ER (calnexin, IRAP, Figure. S2) and endosomal (Rab11) membranes, of primary and 3T3-L1 adipocytes deficient of *Arfrp1* (Figure 2A–D) indicating either ER or endosomal sequestration of the adipokine. Further characterization by immunocytochemical co-stainings of 3T3-L1 adipocytes revealed that intracellular adiponectin was largely immunopositive for recycling endosomal Rab11, an effect that was even more pronounced following *Arfrp1* suppression as evaluated by Pearson's correlation coefficient (Figure 2E,F). Overlap with lysosomal LAMP1 and the TGN marker γ-adaptin was limited (Figure 2E). An intracellular accumulation of leptin after depletion of *Arfrp1* in 3T3-L1 cells by specific siRNA treatment was not observed (Figure S3). Taken together, these results suggest that defective cargo exit from endosomes may retard adiponectin release.

3.3. Loss of *Arfrp1* specifically impairs endosomal-mediated trafficking

Since adiponectin has been described to exit the cell *via* constitutive and regulated pathways involving the endosomal compartment [18],

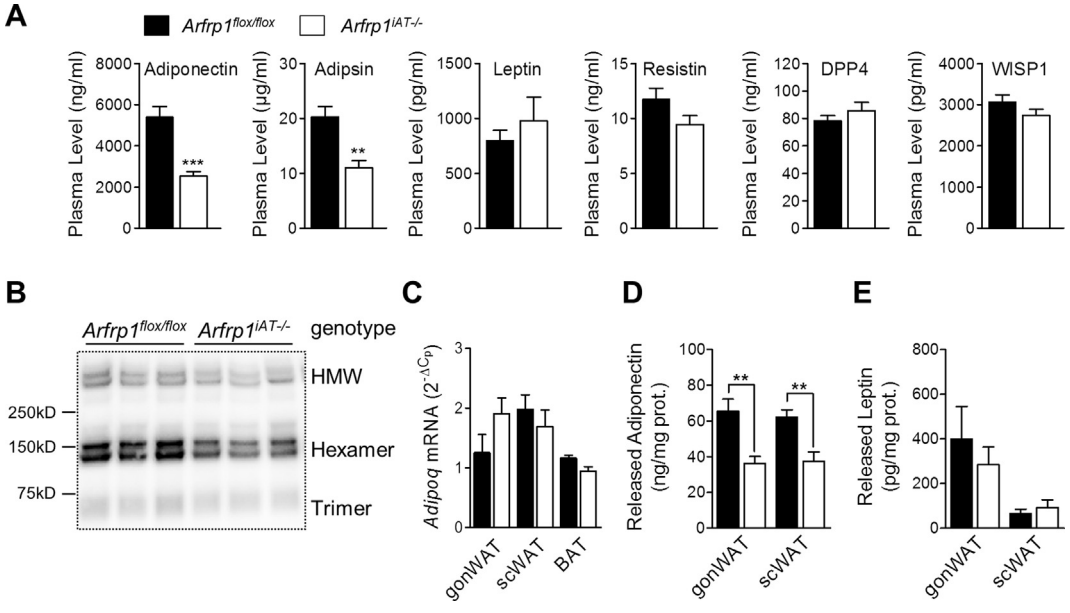

Figure 1: Ablation of *Arfrp1* in adipocytes selectively decreases adiponectin and adipsin secretion. (A) Circulating levels of indicated adipokines detected in plasma of 7-week-old *Arfrp1*$^{iAT-/-}$ (white bars) and control (*Arfrp*$^{flox/flox}$, black bars) mice (n = 5–19 mice per genotype). (B) Adiponectin isoforms measured in plasma of 7-week-old animals. HMW: high molecular weight adiponectin. (C) Adiponectin transcript levels (*Adipoq*) determined in gonadal and subcutaneous white adipose tissue (gonWAT, scWAT) and in brown adipose tissue (BAT) of 7-week-old mice (n = 3–6 mice per genotype). (D, E) Released levels of adiponectin (D) and leptin (E) from gonWAT and scWAT explants of *Arfrp1*$^{iAT-/-}$ and control mice (*n* = 4–6 mice per genotype). All data are presented as mean ± SEM, $^{**}P \leq 0.01$, $^{***}P \leq 0.001$ by unpaired Student's *t*-test.

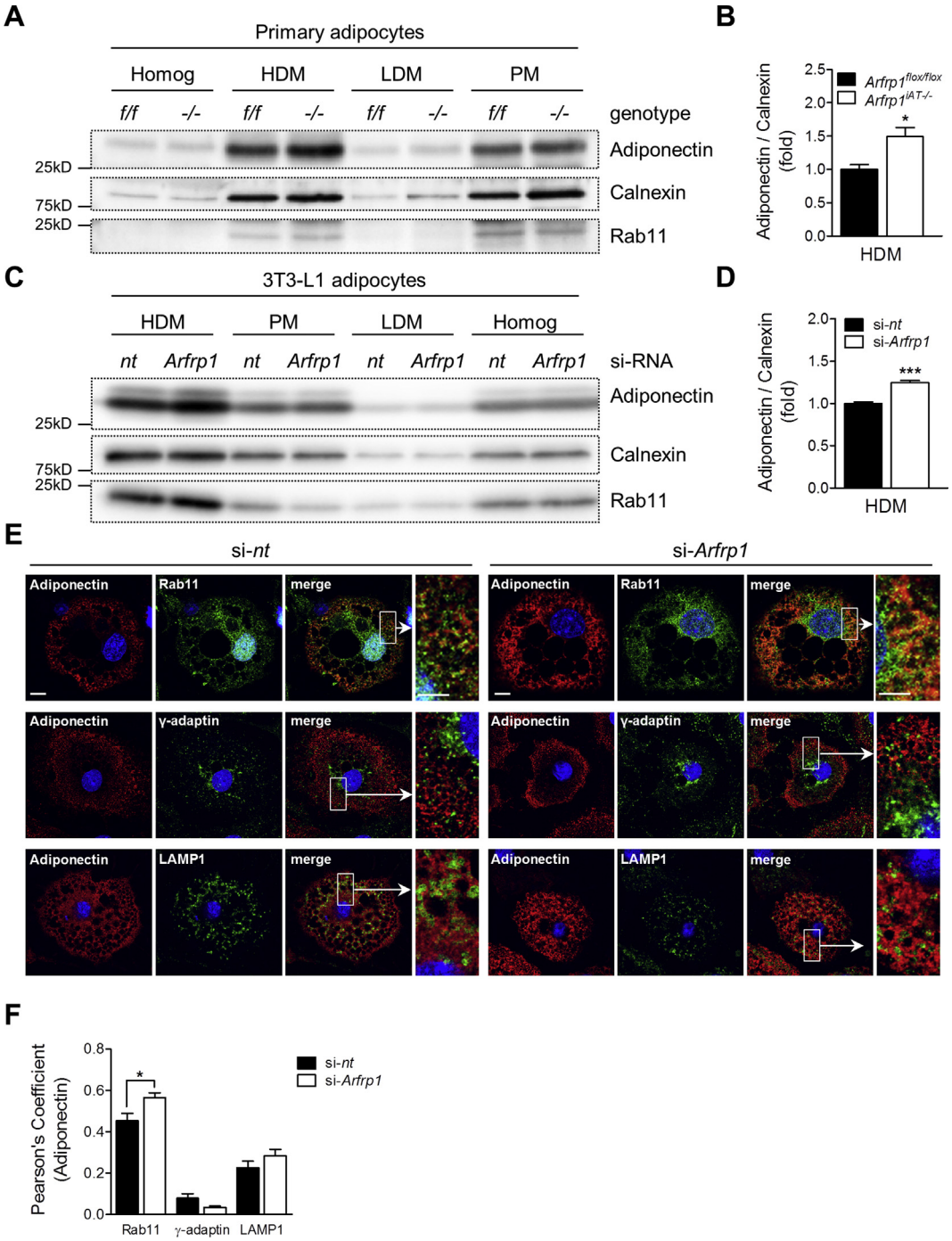

Figure 2: Endosomal accumulation of adiponectin in adipocytes depleted of *Arfrp1*. (A, C) Abundance of adiponectin in subcellular fractions of isolated gonadal adipocytes (gonWAT) from 7-week-old *Arfrp1*$^{iAT-/-}$ (−/−) and *Arfrp*$^{flox/flox}$ mice (*f/f*) (A) and 3T3-L1 adipocytes transfected with *nt* (non-targeting)- or *Arfrp1*-siRNA (C). (B, D) Signal intensities were quantified by densitometric analysis and expressed as fold of control (*Arfrp1*$^{flox/flox}$, si-*nt*) set to 1 (n = 3 independent fractionations). Homog, homogenate; HDM, high-density microsomes; LDM, low-density microsomes; PM, plasma membrane. (C) Transfected 3T3-L1 adipocytes were co-immunostained for adiponectin (red) with either Rab11, γ-adaptin or LAMP1 (green). Scale bar: 10 μm; magnification 5 μm. (F) Quantification of co-localization was calculated by Pearson's correlation coefficient with at least 10−15 images analyzed per condition. Values are presented as mean ± SEM, *$P \leq 0.05$ by unpaired Student's *t*-test.

functionality of both secretory routes was analyzed in the presence and absence of ARFRP1. To trace endocytic and recycling processes, the transferrin receptor (TfR) and its ligand transferrin (Tf), were monitored in *nt*- (non-targeting)- and *Arfrp1*-siRNA transfected HeLa cells. The TfR is internalized after Tf binding at the cell surface and delivered to early endosomes. Thereafter, the Tf-TfR-complex recycles back to the plasma membrane either directly from early endosomes (rapid recycling) or *via* recycling endosomes (slow recycling) [19]. To dissect ARFRP1 function in this context, transfected HeLa cells were incubated with Alexa568-labeled Tf at 37 °C for 30 min to allow receptor-ligand

uptake and recycling. In *Arfrp1*-depleted cells endocytosed Tf—TfR markedly accumulated in close proximity to the plasma membrane, primarily around the cellular tips, whereas control cells displayed Tf—TfR signals throughout the entire cell or concentrated in the perinuclear region as quantified from immunostainings (Figure 3A,B). This result strongly pointed towards an impaired cargo exocytosis from endosomes when ARFRP1 is absent.

In order to monitor Tf—TfR exocytosis, we incubated transfected HeLa cells with Alexa568-Tf at 37 °C for 30 min, removed surface-bound Tf (referred to 0 min) and chased the receptor-ligand release for 20 min. At time point 0 min, endocytosed Tf was markedly lower in *Arfrp1*-depleted cells. However, after 20 min, Tf largely remained intracellularly, whereas most of the Tf was successfully exocytosed from control cells (Figure 3C). Quantification of the relative amount of released Tf (44% vs. 18%) confirmed a significantly impaired exocytosis of Tf-TfR-containing recycling vesicles from *Arfrp1*-knockdown compared to control cells (Figure 3D).

To test whether this results in reduced TfR re-exposure at the plasma membrane, we additionally examined cell surface localization and endocytosis of the TfR and its ligand. Incubation of transfected HeLa cells with Alexa568-conjugated Tf at 4 °C resulted in Tf binding to cell surface-localized TfR (Tf surface), followed by incubation at 37 °C for 5 min allowing clathrin-mediated endocytosis of the Tf-TfR-complex (Tf uptake). In fact, cell surface exposure of the TfR was strikingly reduced by around 45% in cells deficient of ARFRP1 (Figure 3E,F). Accordingly, Tf uptake was markedly lower (44%) upon *Arfrp1* suppression. However, the rate of Tf—TfR endocytosis, calculated by the ratio of Tf uptake to Tf surface, was unaltered (Figure 3F), substantiating the notion that ARFRP1 affects endosomal trafficking at the level of exocytosis rather than being required for endosomal internalization. We next analyzed Tf uptake and recycling in 3T3-L1 adipoocytes in which expression of *Arfrp1* was suppressed by the specific si-RNA. As demonstrated in Figure S4, the release of Tf in si-*Arfrp1* transfected 3T3-L1 cells is reduced which indicates an impaired exocytotic capacity (Figure S4 A, B). Similar to results obtained in HeLa cells, the relative uptake rate was not affected upon *Arfrp1* knockdown (Figure S4 D, E).

As adiponectin was also reported to exit the cell constitutively, we evaluated anterograde cargo trafficking *via* the classical constitutive secretory pathway by applying a HeLa M-C1-based secretion assay [15]. This cell line stably expresses a GFP-tagged reporter construct forming large aggregates, which are trapped within the ER under basal conditions. After the addition of a specific ligand (D/D solubilizer), aggregates are dissolved, allowing the reporter to be transported through the classical secretory pathway in order to be released from cells which was monitored by immunofluorescence microscopy. Although post-Golgi trafficking appeared to be delayed, constitutive secretion in general was intact in *Arfrp1*-depleted HeLa M-C1 cells (Figure S5). Taken together, these data demonstrate that ARFRP1 is required for efficient exocytosis from endosome-derived recycling vesicles, thereby potentially promoting cell surface delivery of certain cargo released *via* the endosomal system such as adiponectin.

3.4. Lack of *Arfrp1* reduces cell surface localization of the insulin receptor

Similar to TfR, the insulin receptor is a transmembrane receptor partially undergoing endocytic recycling following ligand binding and internalization [20,21]. As we detected lower cell surface exposure of the TfR in response to *Arfrp1* suppression, we evaluated the localization of the insulin receptor in adipocytes of 7-week-old $Arfrp1^{iAT-/-}$ and control mice (2 weeks of tamoxifen treatment). Notably, the amount of insulin receptor analyzed in plasma membrane fractions of isolated primary adipocytes from $Arfrp1^{iAT-/-}$ mice was significantly reduced by about 50% compared to plasma membranes of control littermates (Figure 4A,B). At the same time, total insulin receptor levels measured in gonWAT lysates were unaffected (Figure 4C,D). However, following longer *Arfrp1* deletion, at the age of 10 weeks (5 weeks of tamoxifen treatment), the mature receptor was markedly reduced in gonWAT of $Arfrp1^{iAT-/-}$ animals while pro-insulin receptor levels showed no difference between the genotypes, suggesting that insulin receptor mistargeting was followed by its accelerated degradation rather than resulting from transcriptional downregulation. (Figure 4C,D). We confirmed the *in vivo* data by analyzing the subcellular distribution of the insulin receptor in differentiated 3T3-L1 adipocytes. In agreement with membrane fractionations of primary adipocytes, immunocytochemical co-stainings revealed less cell surface localization of the insulin receptor in response to *Arfrp1* suppression (Figure 4E). Accordingly, co-localization of the insulin receptor with the plasma membrane marker caveolin-1, evaluated by Pearson's correlation coefficient, was significantly decreased in *Arfrp1*-depleted cells (Figure 4F). Taken together, we demonstrate that in addition to the TfR in HeLa cells, the insulin receptor in adipocytes was markedly reduced at the plasma membrane, suggesting that ARFRP1 promotes efficient receptor recycling back to the cell surface by regulating endosomal-mediated exocytosis.

3.5. Adipocyte-specific deletion of *Arfrp1* affects insulin response, lipolytic activity, and expandability of adipose tissue

As we found that ARFRP1 is required for an efficient cell surface exposure of the insulin receptor, we tested if adipose insulin sensitivity is impaired in $Arfrp1^{iAT-/-}$ mice. For this purpose, 10-week-old animals were acutely injected with insulin or vehicle (NaCl) and sacrificed 20 min later in order to assess the insulin response of white and brown adipose depots (WAT, BAT). $Arfrp1^{iAT-/-}$ mice revealed a markedly blunted insulin-stimulated AKT phosphorylation in both fat depots, when compared to control littermates (Figure 5A—C). Furthermore, elevated triglyceride, NEFA, and glycerol levels detected in plasma of 10-week-old $Arfrp1^{iAT-/-}$ mice pointed towards an impaired insulin-mediated suppression of adipocyte lipolysis (Figure 5D—F). To evaluate whether impaired adipose insulin signaling of $Arfrp1^{iAT-/-}$ mice caused the alterations in plasma lipid levels, we analyzed *ex vivo* lipolytic activity of gonWAT explants generated from 7-week-old $Arfrp1^{flox/flox}$ and $Arfrp1^{iAT-/-}$ mice. We found that NEFA release from fat biopsies originating from $Arfrp1^{iAT-/-}$ mice was significantly higher than from those of control mice indicating an elevation of basal lipolysis (Figure 5G). Treatment with the β3-adrenergic receptor agonist isoproterenol markedly stimulated NEFA mobilization from explants of both genotypes, however to a lesser extent from those of $Arfrp1^{iAT-/-}$ mice. The addition of insulin failed to suppress isoproterenol-induced lipolysis in explants of $Arfrp1^{iAT-/-}$ mice (Figure 5G) confirming that insulin-mediated inhibition of adipose lipolytic activity was blunted in $Arfrp1^{iAT-/-}$ animals. We also detected ATGL in lysates of control and $Arfrp1^{iAT-/-}$ mice, because insulin has been demonstrated to suppress the expression of the rate-limiting lipolytic enzyme ATGL [22]. The western blots showed a tendency towards higher ATGL levels in gonWAT samples of $Arfrp1^{iAT-/-}$ in comparison to control mice ($p = 0.098$), which is in agreement with the increased basal lipolytic rate observed in these mice (Figures S8A and B). In addition, presumably due to an impaired insulin receptor signaling, $Arfrp1^{iAT-/-}$ mice revealed decreased phospho-FOXO1 levels (Figures S8C and D). In line with that, and with reference to the lipodystrophic phenotype of the conditional fat-specific *Arfrp1* knockout mouse [10], expansion of adipose tissue was found to be impaired in $Arfrp1^{iAT-/-}$ mice

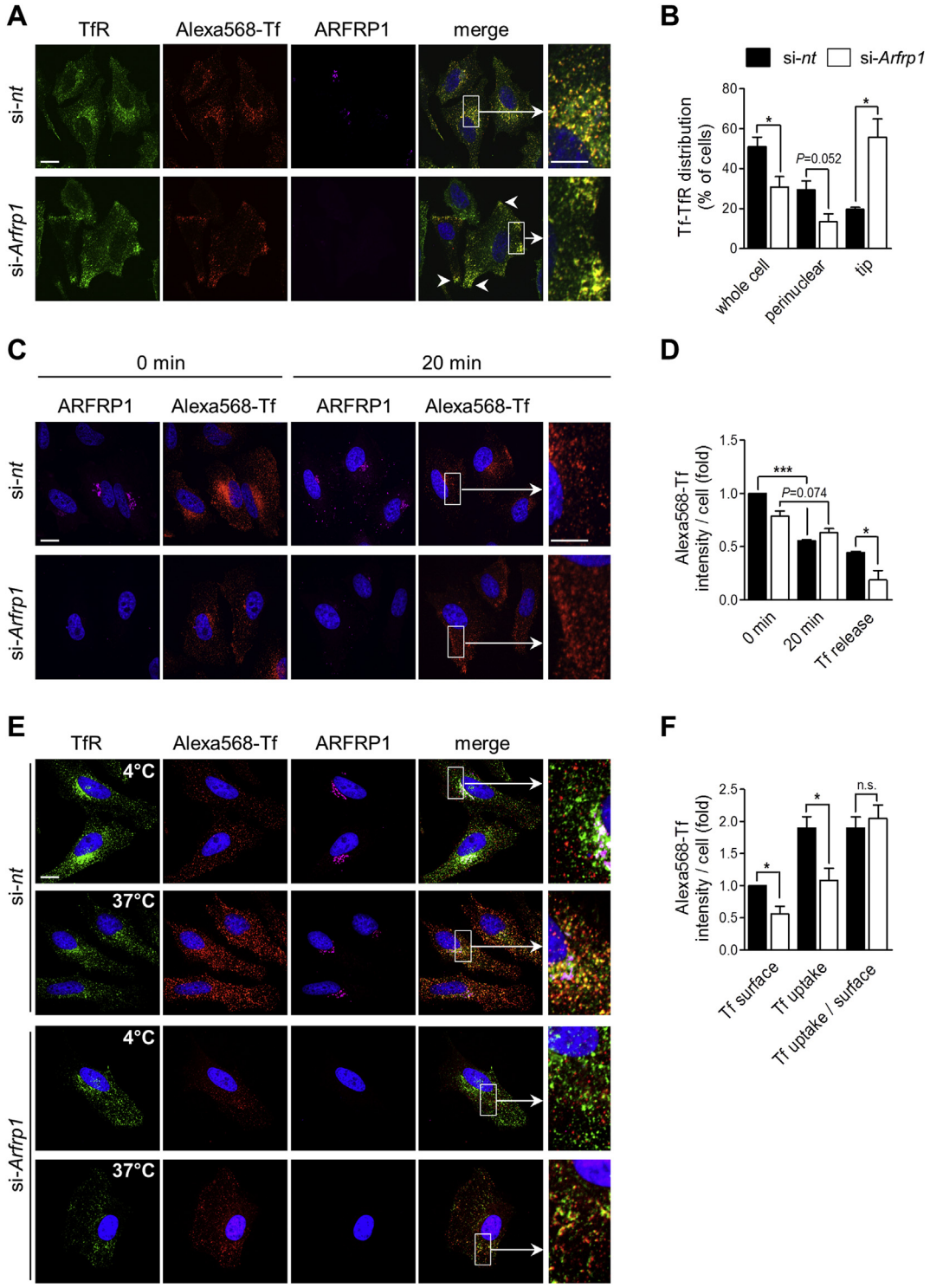

Figure 3: Suppression of *Arfrp1* results in impaired endosomal-mediated secretion at the level of exocytosis. (A) Distribution of the transferrin receptor (TfR, green) and its ligand transferrin (Tf, red) was analyzed in HeLa cells transfected with *nt* (non-targeting, black bars)- or *Arfrp1*-siRNA (white bars) following 30 min of Alexa568-Tf incubation at 37 °C. Cells were co-stained for ARFRP1 (pink). Scale bar: 20 μm. White arrowheads indicate Tf—TfR signals in the tip region. (B) Tf—TfR distribution was classified and counted cells per classification were expressed as percentage of total number of cells. (C, D) Tf—TfR exocytosis was assessed in transfected HeLa cells. At indicated time points, cells were fixed and stained for ARFRP1 (pink) (C). Alexa568-Tf intensity was quantified per cell and expressed as fold of control cells (0 min) set to 1. The relative amount of released Tf was calculated as a measure of Tf—TfR exocytosis (D). (E, F) Tf surface and uptake was analyzed in transfected HeLa cells. Before and after temperature switch, cells were fixed and co-stained with anti-TfR (green) and anti-ARFRP1 (pink) (E). Alexa568-Tf intensity was quantified per cell and expressed as fold of control cells (4 °C) set to 1. The ratio between Tf uptake to Tf surface was calculated as a measure of Tf—TfR endocytosis (F). For all stainings DAPI (blue) was used to visualize nuclei. Scale bar: 20 μm. All quantifications represent mean ± SEM from 3 to 4 independent experiments each with 10—25 images analyzed per condition, n.s. - not significant, $*P \leq 0.05$ by unpaired Student's *t*-test (B, D, F) or by paired *t*-test (D, F).

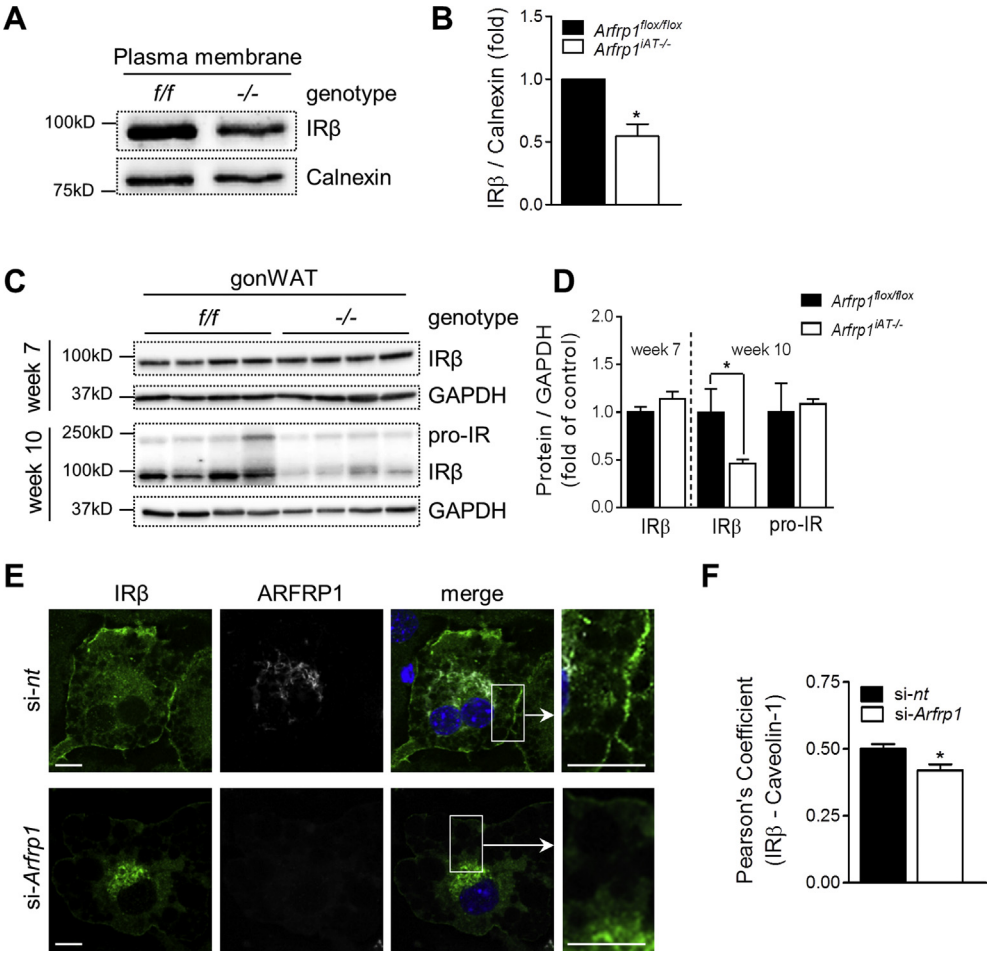

Figure 4: Adipocyte-specific depletion of *Arfrp1* leads to diminished plasma membrane localization of the insulin receptor. (A, B) Abundance of the insulin receptor was assessed by immunoblotting using an antibody against the β subunit (IRβ) in isolated plasma membrane (PM) fractions of gonadal white adipocytes from 7-week-old *Arfrp1*$^{iAT-/-}$ (white bars) and control mice (*Arfrp1*$^{flox/flox}$, black bars) (A). Band intensities were quantified by densitometric analysis and expressed as fold of control set to 1 (n = 3 independent fractionations) (B). (C, D) Analysis of insulin receptor protein levels in gonWAT lysates from 7- and 10-week-old mice by western blotting (C). Signal intensities were quantified by densitometric analysis and expressed as fold of control set to 1 (n = 4–5 mice per genotype) (D). (E) Co-immunostaining of 3T3-L1 adipocytes transfected with *nt* (non-targeting)- or *Arfrp1*-siRNA with antibodies against IRβ (green) and ARFRP1 (white). DAPI (blue) was used to visualize nuclei. Scale bar: 10 μm. (F) Co-localization between insulin receptor and caveolin-1 was quantified by Pearson's correlation coefficient (n = 3 independent transfections). All data are presented as mean ± SEM, *$P \leq 0.05$ by paired *t*-test (B) or by unpaired Student's *t*-test (D, F).

(Figure 5J). As a consequence, body weight gain of these animals was moderately reduced (Figure 5I), whereas development of lean mass was indistinguishable between the genotypes (Figure S6). Histological examination of gonWAT and scWAT sections from 7- and 10-week-old mice (Figure 5L, M) and subsequent quantification of gonadal adipocyte area confirmed that adipocyte enlargement by hypertrophic growth was blunted in *Arfrp1*$^{iAT-/-}$ mice (Figure 5K). From these data, we conclude that reduced cell surface localization of the insulin receptor leads to diminished adipose insulin sensitivity, which, in turn, promotes adipocyte lipolytic activity resulting in attenuation of adipose tissue growth in *Arfrp1*$^{iAT-/-}$ mice. We furthermore conclude that adiponectin release and insulin receptor recycling utilize the same post-Golgi trafficking pathways in adipocytes.

3.6. Adipocyte-specific disruption of *Arfrp1* impairs liver insulin signaling and hepatic control of glucose homeostasis

Since we demonstrated that ARFRP1 is necessary for an adequate secretion of adiponectin, which has insulin-sensitizing properties on peripheral tissues such as liver and skeletal muscle [23,24], we assessed insulin sensitivity of these particular tissues. We found that insulin-stimulated AKT-phosphorylation was dramatically reduced in livers of *Arfrp1*$^{iAT-/-}$ mice, whereas insulin sensitivity of skeletal muscle was unaffected (Figure 6A–C). Adiponectin has been described to enhance hepatic insulin response by an increase in phosphorylation and activity of AMPK [24]; however, the level of phosphorylated AMPK assessed in liver lysates was not different between the genotypes (Figure S7). Beside AMPK-related effects, adiponectin was shown to sensitize the liver towards the action of insulin *via* a selective upregulation of hepatic IRS-2 protein expression [25]. Indeed, we found that IRS-2 protein was significantly diminished in liver lysates of *Arfrp1*$^{iAT-/-}$ compared to control mice (Figure 6D,E), supporting our assumption that deficiency of circulating adiponectin deteriorates hepatic insulin sensitivity of *Arfrp1*$^{iAT-/-}$ animals *via* a selective reduction in hepatic IRS-2 content. In contrast, protein expression of IRS-1 and insulin receptor showed no alterations between the genotypes (Figure 6D,E). Since insulin signaling in the liver largely controls hepatic glucose production, we performed pyruvate tolerance tests following 18 h of fasting. As shown in Figure 6F,G, *Arfrp1*$^{iAT-/-}$ animals displayed considerably higher blood glucose excursions than control littermates, indicating that gluconeogenesis

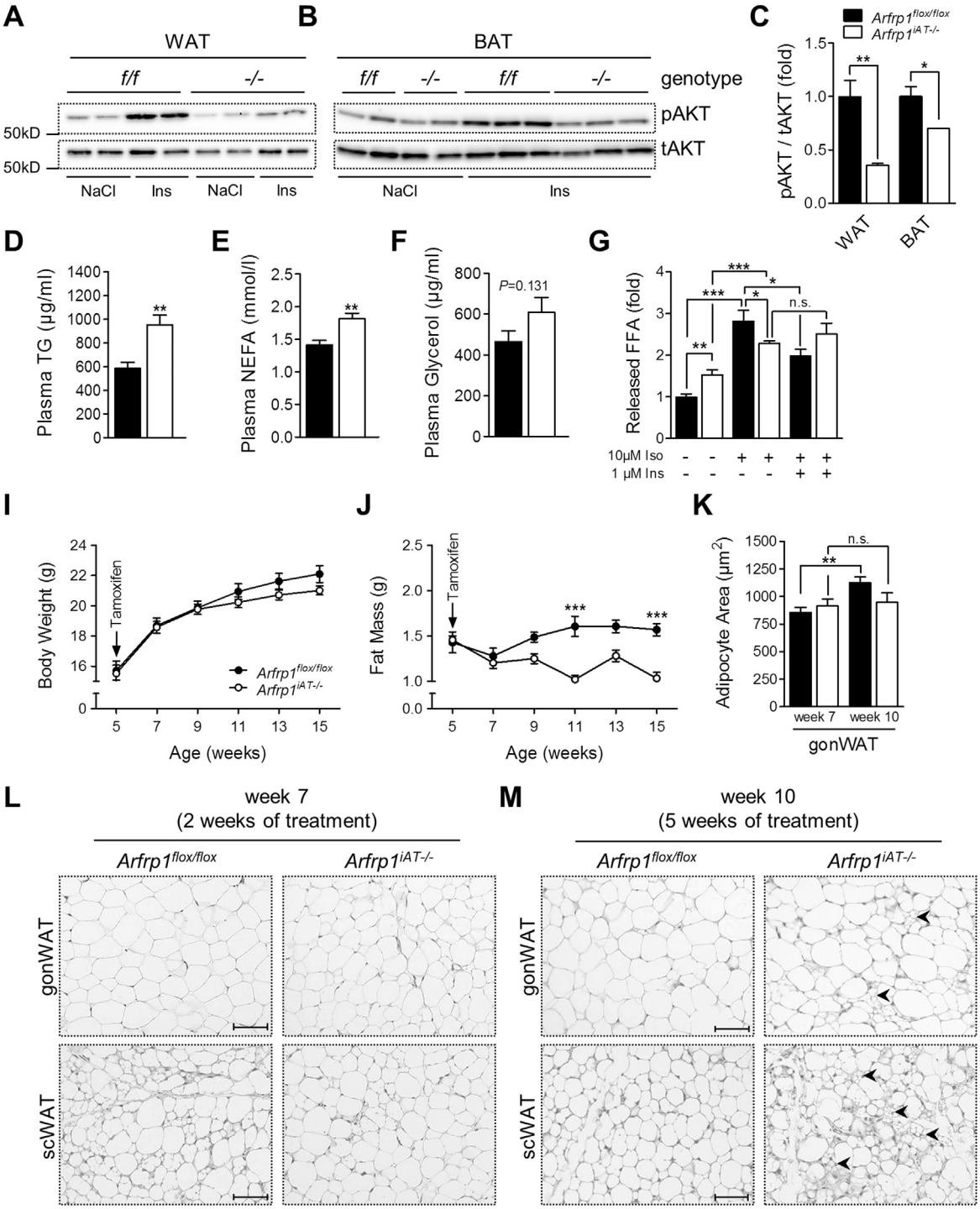

Figure 5: Disruption of *Arfrp1* in adipocytes affects insulin sensitivity, lipolytic rate and expansion of adipose tissue. (A, B) *In vivo* AKT-phosphorylation in subcutaneous white (A) and brown (B) adipose tissue (WAT, BAT) of 10-week-old $Arfrp1^{iAT-/-}$ (−/−; white symbols) and $Arfrp^{flox/flox}$ mice (*f/f*, black symbols) 20 min after injection of insulin (Ins, 1 IU/kg body weight, n = 3–5 mice per genotype) or vehicle (NaCl, n = 2 mice per genotype). (C) Band intensities (insulin treatment) were quantified by densitometric analysis, and the ratio of phosphorylated (pAKT) to total AKT (tAKT) levels was expressed as fold of control set to 1. (D–F) Levels of triglycerides (D), non-esterified fatty acids (NEFA) (E) and glycerol (F) were measured in plasma of 10-week-old mice (n = 10 mice per genotype). (G) *Ex vivo* lipolysis was assessed under indicated conditions in gonadal WAT explants generated from 7-week-old animals by determining NEFA concentration in the supernatant. Data were normalized to corresponding protein content and expressed as fold of untreated controls set to 1 (n = 7–8 mice per genotype). (I, J) Gain of body weight (I) and fat mass (J) of $Arfrp1^{iAT-/-}$ and control mice (n = 14–17 mice per genotype). The arrows indicate start of tamoxifen treatment. (K) Quantification of gonadal adipocyte area from 7- and 10-week-old mice was performed by an automated image analysis software (WimAdipose, Wimasis GmbH) (n = 3–5 mice per genotype and age, each with at least 3 independent histological sections). (L, M) Representative H&E stainings of gonadal and subcutaneous white adipose tissue sections from 7- (L) and 10- (M) week-old animals. Scale bar: 60 µm. Arrowheads indicate areas with smaller adipocytes. All values represent mean ± SEM, n.s. - not significant, $*P \leq 0.05$, $**P \leq 0.01$, $***P \leq 0.001$ by unpaired Student's *t*-test (C-G, K) or by two-way ANOVA with Bonferroni's post-test for multiple comparison (I, J).

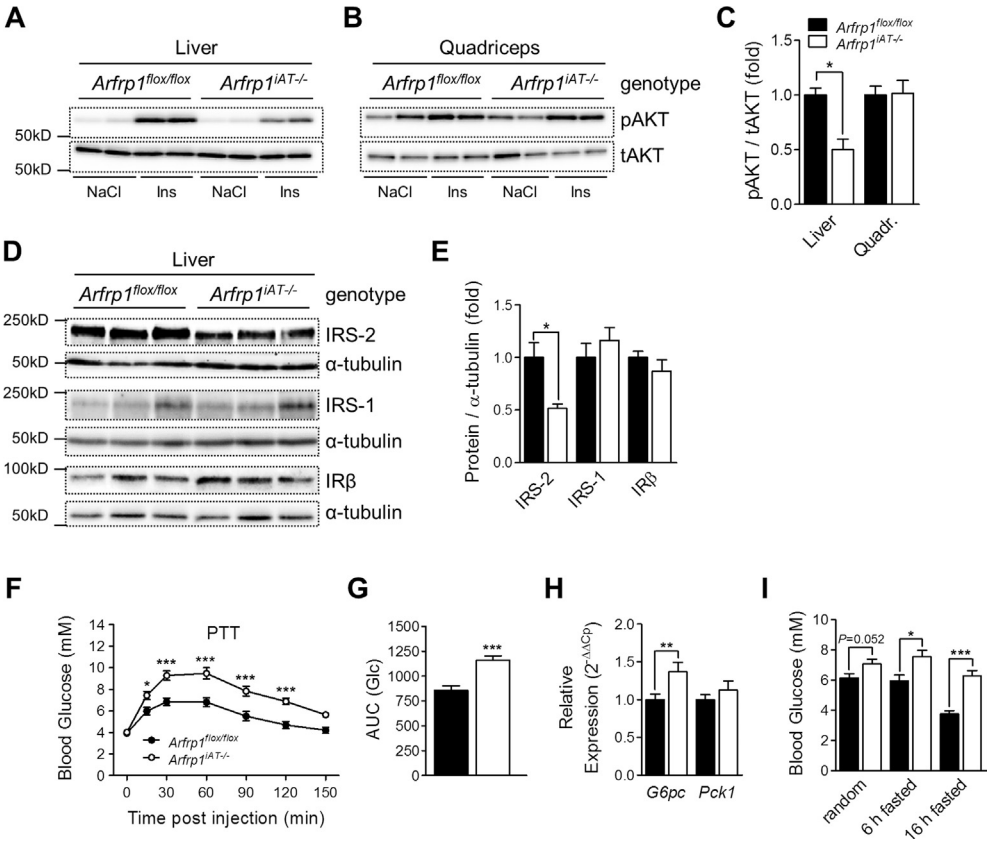

Figure 6: Loss of adipocyte-specific *Arfrp1* results in deteriorated liver insulin sensitivity, increased hepatic glucose production, and elevated fasting blood glucose levels. (A, B) Western blot analysis of phosphorylated (pAKT) and total AKT (tAKT) levels in liver (A) and quadriceps (B) of 10-week-old *Arfrp1*$^{iAT-/-}$ (white symbols) and control mice (*Arfrp1*$^{flox/flox}$, black symbols) following injection with insulin (Ins, 1 IU/kg body weight, n = 3–5 mice per genotype) or vehicle (NaCl, n = 2 mice per genotype). (C) Band intensities (insulin treatment) were quantified by densitometric analysis, and the ratio of pAKT to tAKT was expressed as fold of control set to 1. (D, E) Expression of indicated proteins was determined in liver lysates of 10-week-old animals *via* immunoblotting (D). Signal intensities were quantified by densitometric analysis and expressed as fold of control set to 1 (n = 3–5 mice per genotype) (E). (F) Ten-week-old mice were subjected to pyruvate tolerance tests (PTT), and blood glucose concentration was determined at indicated time points (n = 17–20 animals per genotype). (G) The area under the curve (AUC) is depicted for blood glucose. (H) Transcript levels of gluconeogenic genes (*G6pc*, *Pck1*) were determined by qRT-PCR in livers of 10-week-old animals (n = 4–18 mice per genotype) after 6 h of fasting. (I) Blood glucose concentration was measured in 10-week-old mice at indicated time points (n = 10–17 mice per genotype). All data represent mean ± SEM, $^{*}P \leq 0.05$, $^{**}P \leq 0.01$, $^{***}P \leq 0.001$ by unpaired Student's *t*-test (C, E, G-I) or by two-way ANOVA with Bonferroni's post-test for multiple comparison (F).

was increased in these mice. Accordingly, mRNA expression of *G6pc* was significantly higher in livers of 6 h fasted *Arfrp1*$^{iAT-/-}$ than in control mice further arguing for an elevation in hepatic glucose production *via* gluconeogenesis (Figure 6H). As a consequence, blood glucose concentration was significantly higher in mice lacking *Arfrp1* in adipose tissue after 6 h of fasting, an effect which became even more pronounced after 16 h of food deprivation (Figure 6I). However, it cannot be excluded that the elevated blood glucose concentration in *Arfrp1*$^{iAT-/-}$ mice is also a consequence of an impaired glucose uptake by skeletal muscle and adipose tissue. Taken together, the present data strongly suggest that the impaired release of adiponectin from *Arfrp1*-deficient adipose tissue led to perturbations in the adipo–liver axis. This was characterized by an impaired hepatic insulin sensitivity associated to decreased IRS-2 protein levels, which, in turn, resulted in elevated hepatic gluconeogenesis and increased blood glucose levels in *Arfrp1*$^{iAT-/-}$ mice under fasting conditions.

4. DISCUSSION

In the current study, we have identified adiponectin secretion and insulin receptor surface targeting to largely rely on the action of functional ARFRP1 at the *trans*-Golgi in mature adipocytes. Both cargo molecules utilize *trans*-endosomal routes for cell surface delivery resulting in either secretion (adiponectin) or plasma membrane exposure (insulin receptor). Mice with an inducible deletion of *Arfrp1* in adipocytes reveal significantly less adiponectin release and insulin receptor surface localization causing hepatic insulin resistance and impaired glucose homeostasis as well as reduced adipose insulin signaling promoting lipolytic activity and inhibiting adipose tissue expansion.

Adiponectin, a classically secreted adipokine depending on proper ER/Golgi function, has been reported to exit the cell *via* endosomal-mediated secretion pathways [26]. Initially, folding and assembly of adiponectin into higher-order complexes (trimer, hexamer, high-molecular weight adiponectin) involves a complex set of regulatory steps in the ER and Golgi apparatus [17,27–29]. Once adiponectin reaches the TGN, a pool of adiponectin molecules is packaged into GGA1 (Golgi-localized, gamma adaptin ear containing, ARF-binding protein 1)-coated vesicles for further delivery to endosomes [30]. GGA1 is a monomeric coat adapter known to be activated at the *trans*-Golgi network where it mediates the sorting of selected cargo-containing transport vesicles from the TGN to endosomes [31]. In agreement with that, cellular adiponectin has been shown to partially co-localize with Rab11, a marker of

recycling endosomes as well as with Rab5 and EEA1 (early endosome antigen 1) representing early endosomes [18,32].

Based on assays employing the transferrin receptor (TfR) and its ligand transferrin (Tf), which have been widely used to trace endocytic and recycling processes, we demonstrated in the current study ARFRP1 to be critically involved in the process of endosomal-mediated exocytosis (Figure 3C,D). Consistently, adipocyte-specific ablation of *Arfrp1* in mice (Figure 2A,B) or 3T3-L1 cells (Figure 2C,D) promoted an endosomal enrichment of adiponectin, showing increased co-localization with Rab11-positive recycling endosomes when *Arfrp1* was depleted in 3T3-L1 adipocytes (Figure 2E,F). In accordance with accumulating adiponectin in fat cells, the endosomal transit of the Tf—TfR complex was impaired in *Arfrp1*-deficient HeLa cells as indicated by accumulation of Tf—TfR at the cell periphery in these cells (Figure 3A,B). From these data, we conclude that the loss of *Arfrp1* in adipocytes selectively impairs secretion of adiponectin *via trans*-endosomal routes. Further supportive of this assumption is the finding that a fraction of intracellular adiponectin overlaps with TfR-positive membranes in 3T3-L1 adipocytes, implying that adiponectin release occurs *via* the TfR-positive endosomal compartment [26]. Beside this, adiponectin was also described to exit the cell constitutively [18]. However, this route of secretion is principally intact in *Arfrp1*-depleted cells (Figure S5) and might explain the residual adiponectin that could be detected in plasma and fat explant supernatant of $Arfrp1^{iAT-/-}$ mice.

Notably, both circulating adiponectin and adipsin were equally diminished by about 50% in $Arfrp1^{iAT-/-}$ mice consistent with several studies reporting overlapping trafficking routes for their secretion from 3T3-L1 cells which was strikingly inhibited upon ablation of TfR-positive endosomes [18,26,33]. In agreement with an unaffected leptin secretion (Figure 1A,E), post-Golgi traffic of leptin was shown to occur independently of intact endosomal compartments as their inactivation did not compromise leptin release from 3T3-L1 or primary rat adipocytes [18]. The fact that deletion of *Arfrp1* reduces the plasma levels of adiponectin and adipsin could indicate that the observed phenotype is the consequence of both adipokines. However, the Spiegelman group recently reassessed the metabolic role of adipsin [34] showing that adipsin has an impact on sustaining insulin production and/or secretion particularly under conditions of diet-induced obesity. As mice in the present study received a standard diet and additionally showed no obvious phenotype concerning plasma insulin levels, further investigations focused on adiponectin.

Interestingly, the previously generated conditional fat-specific *Arfrp1* knockout mouse did not exhibit reduced plasma adiponectin levels, as observed in the current study. However, conditional knockout mice failed to develop functional WAT and only displayed residual BAT, still expressing a considerable amount of *Arfrp1*, which might represent the exclusive adiponectin source in these mice [10]. Different mouse models of genetic adiponectin ablation demonstrated a selective hepatic insulin resistance without any impairments of insulin sensitivity in skeletal muscle, even under standard diet-fed conditions [25,35,36]. In this context, hypoadiponectinemia was shown to reduce hepatic IRS-2 expression [20,31]. In particular, adiponectin transiently increases macrophage-derived plasma IL-6 levels, which, in turn, activate hepatic STAT3 to induce hepatic IRS-2 expression and enhance insulin sensitivity in the liver [20]. Intriguingly, IRS-2 largely determines insulin signaling in the liver during fasting, thereby substantially controlling hepatic glucose production *via* gluconeogenesis [21].

These findings conclusively connect the plasma adiponectin decline to the impaired hepatic control of glucose homeostasis in these animals. Following defective endosomal-mediated exocytosis, cell surface exposure of the TfR was substantially diminished in *Arfrp1*-depleted HeLa cells (Figure 3E,F). Similarly, the insulin receptor was less abundant at the plasma membrane in primary adipocytes (Figure 4A,B) and 3T3-L1 cells (Figure 4E,F) deficient of *Arfrp1*. After binding of insulin to its receptor and internalization, receptor-ligand complexes are directed for either lysosomal degradation, a way of downregulating signal reception, or receptors are sorted for reinsertion into the plasma membrane [37,38]. In this context, it was demonstrated that prevention of insulin receptor recycling resulted in an accelerated shunting to a degradative pathway, thereby reducing the amount of total cellular receptors [21]. Indeed, 10-week-old $Arfrp1^{iAT-/-}$ mice revealed substantially diminished protein levels of the mature receptor in gonWAT lysates, suggesting that impaired re-exposure at the cell surface, as assessed by lower plasma membrane abundance in adipocytes from 7-week-old $Arfrp1^{iAT-/-}$ mice, was accompanied by enhanced receptor degradation (Figure 4C,D).

As expected, the insulin receptor surface deficiency resulted in reduced adipose insulin sensitivity (Figure 5A—C). By promoting triglyceride synthesis and inhibiting lipolysis, insulin signaling enhances overall lipid storage in adipocytes. Consistently, adipose tissue explants from $Arfrp1^{iAT-/-}$ mice exhibited an increased basal lipolytic rate as well as impaired insulin-mediated suppression of isoproterenol-stimulated lipolysis (Figure 5G). Insufficiently repressed lipolysis consequently associated with an impaired hypertrophic growth of adipose tissue depots in $Arfrp1^{iAT-/-}$ mice (Figure 5J). Collectively, these findings demonstrate the requirement of ARFRP1 for mature adipocytes to maintain proper insulin action, thereby determining adipose tissue mass. The importance of insulin in controlling lipolysis and fat mass is further emphasized by mouse models with alterations in the insulin signaling pathway of adipocytes. For example, mice with a tamoxifen-inducible knockout of the insulin receptor in mature adipocytes reveal a substantial decrease of adipose tissue mass due to increased lipolysis and adipocyte apoptosis resembling most of the features of the $Arfrp1^{iAT-/-}$ phenotype [39]. Furthermore, the sorting receptor SORLA was recently identified to interact with the insulin receptor in adipocytes facilitating its redirection to the cell surface and enhancing insulin signal reception. Accordingly, mice overexpressing SORLA specifically in adipocytes revealed higher insulin receptor surface levels and decreased lipolysis, which promotes the acquisition of fat tissue and exacerbates diet-induced obesity, while SORLA knockout mice showed excessive lipolysis and a reduction in WAT mass [40].

Notably, numerous genetic variants encoding proteins involved in vesicular transportation (e.g. ARL15, Hip1, Rab3gap1) have been identified by genome-wide association studies (GWAS) as being associated with type 2 diabetes-related traits in humans [41]. These findings further highlight the relevance of functional intracellular vesicle trafficking in preserving metabolic health.

5. CONCLUSIONS

Collectively, the present study suggests that adiponectin secretion and insulin receptor surface targeting share the same post-Golgi trafficking pathways which are regulated by the ARFRP1-based sorting machinery. In this regard, our results underline the pivotal role of ARFRP1 for mature adipocytes in maintaining adipose tissue mass and glucose homeostasis.

FUNDING

This work was supported by the German Ministry of Education and Research and the Brandenburg State (BMBF; DZD grant 82DZD00302) and by the German Research Foundation (DFG; SFB 958).

AUTHOR CONTRIBUTIONS

M.R., D.H., and A.S. performed study conception and design; M.R., M.M.W., I.W., C.B., D.H., and K.S. performed research; M.R., M.M.W., I.W., M.K. analyzed and interpreted data; N.W. and S.O. provided *Adipoq*CreER^{T2} mice; M.R. and A.S. wrote the manuscript.

ACKNOWLEDGEMENTS

The skillful technical assistance of Andrea Teichmann, Anett Helms, and Sarah Ernst from the German Institute of Human Nutrition Potsdam-Rehbruecke is gratefully acknowledged.

CONFLICT OF INTEREST

All authors declare no conflict of interest.

APPENDIX A. SUPPLEMENTARY DATA

Supplementary data related to this article can be found at https://doi.org/10.1016/j.molmet.2017.11.011.

REFERENCES

[1] Rodriguez-Boulan, E., Müsch, A., 2005. Protein sorting in the Golgi complex: shifting paradigms. Biochimica et Biophysica Acta (BBA) — Molecular Cell Research 1744(3):455—464.

[2] Gillingham, A.K., Munro, S., 2007. The small G proteins of the Arf family and their regulators. Annual Review of Cell and Developmental Biology 23(1):579—611.

[3] Burd, C.G., Strochlic, T.I., Gangi Setty, S.R., 2004. Arf-like GTPases: not so Arf-like after all. Trends in Cell Biology, 687—694.

[4] Shin, H.-W., Kobayashi, H., Kitamura, M., Waguri, S., Suganuma, T., Uchiyama, Y., et al., 2005. Roles of ARFRP1 (ADP-ribosylation factor-related protein 1) in post-Golgi membrane trafficking. Journal of Cell Science, 4039—4048.

[5] Nishimoto-Morita, K., Shin, H.-W., Mitsuhashi, H., Kitamura, M., Zhang, Q., Johannes, L., et al., 2009. Differential effects of depletion of ARL1 and ARFRP1 on membrane trafficking between the trans-Golgi network and endosomes. The Journal of Biological Chemistry 284(16):10583—10592.

[6] Zahn, C., Jaschke, A., Weiske, J., Hommel, A., Hesse, D., Augustin, R., et al., 2008. ADP-ribosylation factor-like GTPase ARFRP1 is required for trans-Golgi to plasma membrane trafficking of E-cadherin. The Journal of Biological Chemistry 283(40):27179—27188.

[7] Guo, Y., Zanetti, G., Schekman, R., 2013. A novel GTP-binding protein-adaptor protein complex responsible for export of Vangl2 from the trans Golgi network. eLife, 1—21.

[8] Hesse, D., Hommel, A., Jaschke, A., Moser, M., Bernhardt, U., Zahn, C., et al., 2010. Altered GLUT4 trafficking in adipocytes in the absence of the GTPase Arfrp1. Biochemical and Biophysical Research Communications 394(4):896—903.

[9] Hesse, D., Jaschke, A., Kanzleiter, T., Witte, N., Augustin, R., Hommel, A., et al., 2012. GTPase ARFRP1 is essential for normal hepatic glycogen storage and insulin-like growth factor 1 secretion. Molecular and Cell Biology 32(21):4363—4374.

[10] Hommel, A., Hesse, D., Völker, W., Jaschke, A., Moser, M., Engel, T., et al., 2010. The ARF-like GTPase ARFRP1 is essential for lipid droplet growth and is involved in the regulation of lipolysis. Molecular and Cellular Biology, 1231—1242.

[11] Indra, A.K., Warot, X., Brocard, J., Bornert, J.M., Xiao, J.H., Chambon, P., et al., 1999. Temporally-controlled site-specific mutagenesis in the basal layer of the epidermis: comparison of the recombinase activity of the tamoxifen-inducible Cre-ER(T) and Cre-ER(T2) recombinases. Nucleic Acids Research 27(22):4324—4327.

[12] Sassmann, A., Offermanns, S., Wettschureck, N., 2010. Tamoxifen-inducible Cre-mediated recombination in adipocytes. Genesis 48(10):618—625.

[13] Joost, H.-G., Schürmann, A., 2001. Subcellular fractionation of adipocytes. Adipose tissue protocols, vol. 155. New Jersey: Humana Press. p. 077—82.

[14] Schwenk, R.W., Jonas, W., Ernst, S.B., Kammel, A., Jähnert, M., Schürmann, A., 2013. Diet-dependent alterations of hepatic Scd1 expression are accompanied by differences in promoter methylation. Hormone and Metabolic Research 45(11):786—794.

[15] Gordon, D.E., Bond, L.M., Sahlender, D.A., Peden, A.A., 2010. A targeted siRNA screen to identify SNAREs required for constitutive secretion in mammalian cells. Traffic 11(9):1191—1204.

[16] Ketel, K., Krauss, M., Nicot, A.-S., Puchkov, D., Wieffer, M., Müller, R., et al., 2016. A phosphoinositide conversion mechanism for exit from endosomes Phosphoinositides are a minor class of short-lived membrane phospholipids that serve crucial functions in cell physiology ranging from cell signalling and motility to their role as signposts. Nature 529.

[17] Wang, Z.V., Schraw, T.D., Kim, J.Y., Khan, T., Rajala, M.W., Follenzi, A., et al., 2007. Secretion of the adipocyte-specific secretory protein adiponectin critically depends on thiol-mediated protein retention. Molecular and Cellular Biology, 3716—3731.

[18] Xie, L., O'Reilly, C.P., Chapes, S.K., Mora, S., 2008. Adiponectin and leptin are secreted through distinct trafficking pathways in adipocytes. Biochimica et Biophysica Acta - Molecular Basis of Disease, 99—108.

[19] Mayle, K.M., Le, A.M., Kamei, D.T., 2012. The intracellular trafficking pathway of transferrin. Biochimica et Biophysica Acta 1820(3):264—281.

[20] Marshall, S., Olefsky, J.M., 1983. Separate intracellular pathways for insulin receptor recycling and insulin degradation in isolated rat adipocytes. Journal of Cellular Physiology 117(2):195—203.

[21] Marshall, S., 1985. Kinetics of insulin receptor internalization and recycling in adipocytes. Shunting of receptors to a degradative pathway by inhibitors of recycling. The Journal of Biological Chemistry 260(7):4136—4144.

[22] Chakrabarti, P., Kandror, K.V., 2009. FoxO1 controls insulin-dependent adipose triglyceride lipase (ATGL) expression and lipolysis in adipocytes. The Journal of Biological Chemistry 284(20):13296—13300.

[23] Combs, T.P., Berg, A.H., Obici, S., Scherer, P.E., Rossetti, L., 2001. Endogenous glucose production is inhibited by the adipose-derived protein Acrp30. Journal of Clinical Investigation 108(12):1875—1881.

[24] Yamauchi, T., Kamon, J., Minokoshi, Y., Ito, Y., Waki, H., Uchida, S., et al., 2002. Adiponectin stimulates glucose utilization and fatty-acid oxidation by activating AMP-activated protein kinase. Nature Medicine 8(11):1288—1295.

[25] Awazawa, M., Ueki, K., Inabe, K., Yamauchi, T., Kubota, N., Kaneko, K., et al., 2011. Adiponectin enhances insulin sensitivity by increasing hepatic IRS-2 expression via a macrophage-derived IL-6-dependent pathway. Cell Metabolism 13(4):401—412.

[26] Clarke, M., Ewart, M.A., Santy, L.C., Prekeris, R., Gould, G.W., 2006. ACRP30 is secreted from 3T3-L1 adipocytes via a Rab11-dependent pathway. Biochemical and Biophysical Research Communications 342(4):1361—1367.

[27] Wang, Y., Lam, K.S.L., Chan, L., Chan, K.W., Lam, J.B.B., Lam, M.C., et al., 2006. Post-translational modifications of the four conserved lysine residues within the collagenous domain of adiponectin are required for the formation of its high molecular weight oligomeric complex. Journal of Biological Chemistry 281(24):16391—16400.

[28] Wang, Z.V., Scherer, P.E., 2008. DsbA-L is a versatile player in adiponectin secretion. Proceedings of the National Academy of Sciences 105(47):18077—18078.

[29] Wang, Z.V., Scherer, P.E., 2016. Adiponectin, the past two decades. Journal of Molecular Cell Biology 8(2):93—100.

[30] Xie, L., Boyle, D., Sanford, D., Scherer, P.E., Pessin, J.E., Mora, S., 2006. Intracellular trafficking and secretion of adiponectin is dependent on GGA-coated vesicles. The Journal of Biological Chemistry 281(11):7253—7259.

[31] Takatsu, H., Katoh, Y., Shiba, Y., Nakayama, K., 2001. Golgi-localizing, gamma-adaptin ear homology domain, ADP-ribosylation factor-binding (GGA) proteins interact with acidic dileucine sequences within the cytoplasmic domains of sorting receptors through their Vps27p/Hrs/STAM (VHS) domains. The Journal of Biological Chemistry 276(30):28541—28545.

[32] Carson, B.P., Del Bas, J.M., Moreno-Navarrete, J.M., Fernandez-Real, J.M., Mora, S., 2013. The rab11 effector protein FIP1 regulates adiponectin trafficking and secretion. PLoS One e74687.

[33] Millar, C.A., Meerloo, T., Martin, S., Hickson, G.R.X., Shimwell, N.J., Wakelam, M.J.O., et al., 2000. Adipsin and the glucose transporter GLUT4 traffic to the cell surface via independent pathways in adipocytes. Traffic 1(2):141—151.

[34] Lo, J.C., Ljubicic, S., Leibiger, B., Kern, M., Leibiger, I.B., Moede, T., et al., 2014. Adipsin is an adipokine that improves β cell function in diabetes. Cell 158(1):41—53.

[35] Nawrocki, A.R., 2005. Mice lacking adiponectin show decreased hepatic insulin sensitivity and reduced responsiveness to peroxisome proliferator-activated receptor agonists. The Journal of Biological Chemistry 281(5): 2654—2660.

[36] Yano, W., Kubota, N., Itoh, S., Kubota, T., Awazawa, M., Moroi, M., et al., 2008. Molecular mechanism of moderate insulin resistance in adiponectin-knockout mice. Endocrine Journal, 515—522.

[37] Fan, J.Y., Carpentier, J.L., Gorden, P., Van Obberghen, E., Blackett, N.M., Grunfeld, C., et al., 1982. Receptor-mediated endocytosis of insulin: role of microvilli, coated pits, and coated vesicles. Proceedings of the National Academy of Sciences of the United States of America 79(24):7788—7791.

[38] Fagerholm, S., Örtegren, U., Karlsson, M., Ruishalme, I., Strålfors, P., 2009. Rapid insulin-dependent endocytosis of the insulin receptor by caveolae in primary adipocytes. PLoS One 4(6):e5985.

[39] Sakaguchi, M., Fujisaka, S., Cai, W., Winnay, J.N., Konishi, M., O'Neill, B.T., et al., 2017. Adipocyte dynamics and reversible metabolic syndrome in mice with an inducible adipocyte-specific deletion of the insulin receptor. Cell Metabolism, 1—15.

[40] Schmidt, V., Schulz, N., Yan, X., Schürmann, A., Kempa, S., Kern, M., et al., 2016. SORLA facilitates insulin receptor signaling in adipocytes and exacerbates obesity. Journal of Clinical Investigation 126(7):18—24.

[41] Kluth, O., Matzke, D., Schulze, G., Schwenk, R.W., Joost, H.-G., Schurmann, A., 2014. Differential transcriptome analysis of diabetes-resistant and -sensitive mouse islets reveals significant overlap with human diabetes susceptibility genes. Diabetes 63(12):4230—4238.

